## Invading activity fronts stabilize excitable systems against stochastic extinction

Kenneth A. V. Distefano,\* Sara Shabani,† and Uwe C. Täuber †
Department of Physics (MC 0435) & Center for Soft Matter and Biological Physics,
Robeson Hall, 850 West Campus Drive, Virginia Tech, Blacksburg, VA 24061

(Dated: November 17, 2025)

Stochastic chemical reaction or population dynamics in finite systems often terminates in an absorbing state. Yet in large spatially extended systems, the time to reach species extinction (or fixation) becomes exceedingly long. Tuning control parameters may diminish the survival probability, rendering species coexistence susceptible to stochastic extinction events. In inhomogeneous settings, where a vulnerable subsystem is diffusively coupled to an adjacent stable patch, the former is reanimated through continuous influx from the interfaces, provided the absorbing region sustains spreading activity fronts. We demonstrate this generic elimination of finite-size extinction instabilities via immigration flux in predator-prey, epidemic spreading, and cyclic competition models.

Stochastic dynamics captures the essence of many processes in nature, at least on a coarse-grained description level. In genuine non-equilibrium physical, chemical, and biological systems, absorbing states play a prominent role [1]. Once such a configurations is reached, the transition rate to any other state vanishes. Consequently, the stochastic kinetics ceases and escape from an absorbing state is impossible. Prominent examples are inert compounds in chemical kinetics [2]; population extinction or fixation in ecology [3, 4]; pathogen eradication or full immunity in epidemiology [5]; but also trapped configurations in constrained or disordered physical systems [6–8]; and certain dynamical phases in fluid turbulence [9, 10].

Any finite stochastic system featuring one or more absorbing states will ultimately terminate there. Chemical activity, species coexistence, and epidemic outbreaks are thus fundamentally transient phenomena. However, mean times  $t_{\rm ext}$  to reach extinction or fixation typically grow exponentially with system size, i.e., the number of constituents N:  $t_{\rm ext}(N) \sim e^{cN}$  [11, 12]. In practice, therefore, stochastic trajectories in large enough systems that are initiated at sufficient separation from an absorbing state become highly unlikely to ever reach it. Moreover, in spatially extended systems [13] spreading activity fronts tend to locally trigger excitations and facilitate escape from absorbing states [14]. Thus, mean extinction times are drastically prolonged, and in effect, sufficiently big systems display persistent activity for any experimentally reasonable or computationally accessible time scales  $t < t_{\rm ext}$ . Indeed, many prominent (mean-field) reactiondiffusion models sustain invasion fronts that propagate from either localized or extended active sources into dormant inactive regions [15, 16]. In stochastic spatial reactive systems, demographic fluctuations may excite robust dynamical noise-induced Turing patterns [17–21].

Taking first the thermodynamic limit  $N \to \infty$  followed by  $t \to \infty$ , one may encounter the scenario that upon changing a relevant control parameter (e.g., reaction, reproduction, predation, or infection rates) a genuine dynamical phase transitions occurs (in the infinite system) that separates an active stationary phase from an inac-

tive, absorbing configuration. Since the latter manifestly violates micro-reversibility and detailed balance, such active-to-absorbing state transitions are situated away from thermal equilibrium. On regular spatial lattices, they are generically continuous and universally governed by the scaling exponents of critical directed percolation (DP) [19, 22–27], even in multi-species systems [28]. Typical examples are the contact process [29, 30] or stochastic susceptible-infectious-susceptible (SIS) epidemic model on a lattice [5] and the stochastic spatial Lotka-Volterra (LV) predator-prey or pathogen-host competition model [31, 32] with finite prey carrying capacity K that causes a predator extinction threshold [17, 20, 33–35]. Exceptions involve higher-order processes beyond binary reactions, the presence of additional conserved (diffusive) modes, and/or persistent memory effects that imply temporal non-locality [19, 24–26]. For example, the epidemic threshold in the susceptible-infectious-recovered (SIR) model [5, 15, 36] is characterized by the *dynamic* isotropic percolation (DIP) universality class [37–39].

Thus, in nonlinear stochastic systems, one may observe two distinct types of extinction or fixation "transitions": (i) Genuine active-to-absorbing state phase transitions that require taking the thermodynamic limit  $N \to \infty$ first, then  $t \to \infty$  and tuning appropriate control parameters. They display only a weak dependence of the transition point on N through standard finite-size scaling. (ii) Stochastic extinction events in finite "small" systems, triggered by temporal trajectories that randomly reach an absorbing state. These are highly sensitive to the system size N, potentially to the chosen initial conditions, and often to system control parameters. Upon increasing N, the extinction probability rapidly decreases and indeed vanishes in the thermodynamic limit, where a persistent active phase prevails. Consequently, type (ii) extinction or fixation events technically are "finitesize" phenomena; yet they often feature prominently in real complex biological, ecological, chemical, and physical systems. This is exemplified in Fig. 1(a), which shows both the "true" type (i) predator extinction phase transition and strongly size-dependent type (ii) total popula-

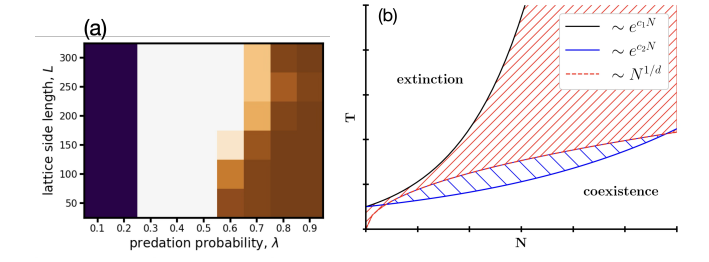


FIG. 1. (a) Coexistence (white), prey fixation (dark blue) and total extinction (with increasing probability indicated in darker brown shades) regimes in the stochastic LV model on a  $L \times L$  square lattice as function of L and the predation probability  $\lambda$  (with fixed  $\mu = 0.1$ ,  $\sigma = 0.2$ , and K = 3). The (largely) size-independent genuine (DP) predator extinction transition of type (i) occurs at  $\lambda_c \approx 0.3$ . For large  $\lambda > 0.5$ , one observes stochastic type (ii) total population extinction events with strongly L-dependent probability [40, 41]. (b) Schematic dependence on system size N of invasion front traversal  $t_{\rm inv} \sim$  $N^{1/d}$  (red dashed) and mean extinction times  $t_{\rm ext}$  for robust (black,  $c_1 > c_2$ ) and vulnerable (blue) (sub-)systems prone to be stochastically driven into an absorbing state. For  $t_{\text{ext},1} >$  $t > t_{\rm inv}$  (shaded red), an excitable patch subject to stochastic extinction for  $t > t_{\text{ext},2}$  (shaded blue) may be reanimated and stabilized via diffusive coupling to an active region.

tion extinction at large predation efficacies in a LV model simulated on a square lattice of linear size L [40, 41].

Spatially inhomogeneous systems consisting of, e.g., diffusively coupled regions set in distinct macroscopic phases separated by type (i) genuine phase transitions remain essentially separated: Their mutual influence is limited to the vicinity of the interfaces between the subsystems, on the scale of the respective characteristic correlation lengths. This is manifest, for example, in checkerboard LV model patches alternatingly situated in the two-species coexistence phase and the predator extinction regime [42], and in similarly coupled subsystems comprising two different cyclic three-species competition models [3, 4], namely the "rock-paper-scissors" and May-Leonard (ML) [43] variants [44]. In contrast, in this letter we demonstrate that diffusively coupling two finite regions that are respectively vulnerable to and robust against type (ii) stochastic extinction or fixation events, induces activity influx across the system interfaces from the stable patch. If the inactive state sustains traveling invasion fronts, these subsequently reinvigorate the entire unstable region and persistently render it immune to reaching the absorbing state, even if the incitatory patch is much smaller in its spatial extent than the vulnerable region. Thus stochastic extinction events are countermanded by another finite-size effect, namely population influx through the interfaces. The robust patch merely needs to remain in a stable active state itself and stay in contact with the vulnerable subsystem until the invasion fronts have permeated deeply enough; the in isolation extinction-prone region is then characterized by the

same macroscopic spatio-temporal features that it would display if its extension were increased sufficiently to move it towards large extinction times  $t_{\text{ext}} \gg t$ .

The qualitative picture is schematically outlined in Fig. 1(b): Stabilization of the vulnerable region (2) is attainable for simulation (or experiment) run times  $t < t_{\rm ext,1} \sim e^{c_1 N_1}$ , the stable patch's (1) mean extinction time (black curve). Beyond the weaker ecology's extinction time  $t > t_{\rm ext,2} \sim e^{c_2 N_2}$  ( $0 < c_2 < c_1$ , blue line), activity in the vulnerable region will have ceased. Traveling immigration waves (front speed v) originating at both interfaces with the stable patch will traverse through the inactive region of perpendicular width  $L_{\perp}$  by the characteristic time  $t_{\rm inv} \approx L_{\perp}/2v \sim N_2^{1/d}$  (red-dashed). During the "transient" window  $t_{\rm inv} < t < t_{\rm ext,1}$ , stochastic extinction (or fixation) in region 2 is countermanded by the influx from region 1, irrespective of its width  $L_{\perp}$ .

We first illustrate this general stabilization mechanism in the simplest hierarchical population dynamics consisting of just two competing species, namely the LV model defined through the stochastic processes predator (pathogen) death  $I \to \emptyset$ , prey (host) reproduction (branching)  $S \to S + S$ , and the predation (infection) reaction  $S + I \rightarrow I + I$ , respectively with probabilities (or positive rates, per unit time)  $\mu$ ,  $\sigma$ , and  $\lambda$ . On a regular square lattice with periodic boundary conditions, we impose a finite local carrying capacity restricting all site-i occupation numbers to  $n_i = n_{Si} + n_{Ii} \leq K$ . The algorithm employed in this work places prey offspring adjacent to their parent's location i provided  $n_i \leq K-1$ there, thus inducing diffusive propagation. The binary predation reaction requires both S and I individuals to be simultaneous present either on the same or a nearestneighbor site. The simulation advances through random sequential updates. A Monte Carlo step (MCS) is completed when on average every particle had the chance to undergo a reaction [17, 20, 21]. We set  $\mu = 0.1$ ,  $\sigma = 0.2$ , and  $\lambda = 0.9$ ; for carrying capacity K = 1, systems of linear size L = 100 or larger then display species coexistence throughout the simulation runs, irrespective of their initialization. In contrast, for K=3 and a random (Poisson) initial particle placement at sufficiently large starting density, early-time large-amplitude local population spikes tend to drive the system stochastically to one of its absorbing states (typically total extinction rather than prey fixation) even at L = 200 [40, 41].

With the above fixed reaction parameters, we construct a spatially inhomogeneous setup where a stable LV two-species coexistence environment with K=1 is placed in diffusive contact with a vulnerable ecology with K=3: Once a particle attempts to cross either of the two interfaces to the other region, it is subject to the carrying capacity there. The simulation snapshots in Fig. 2(a)-(d) depict the ensuing dynamics in a typical realization: Beginning with a random particle distribution, the smaller  $(200 \times 100)$  stable region quickly develops the character-

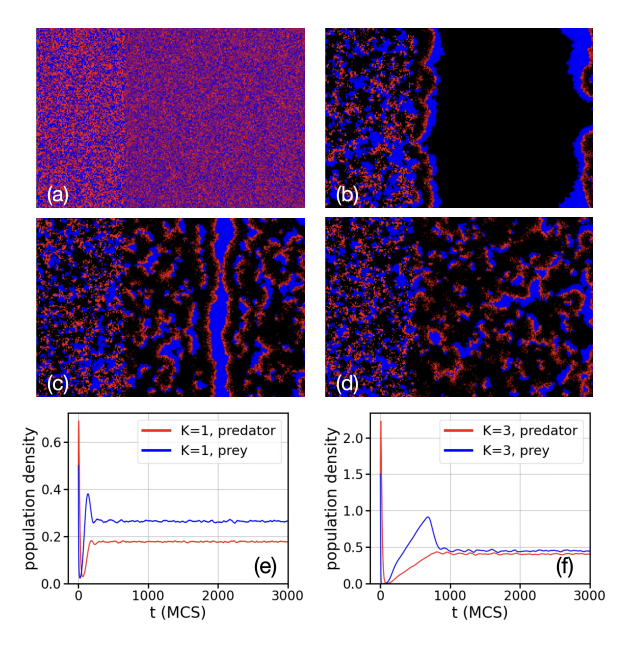


FIG. 2. Snapshots of a single Monte Carlo simulation run for two diffusively coupled LV systems on a square lattice (height  $L_{\parallel} = 200$ , periodic boundary conditions), (a) initialized (t = 0) with a random distribution of single predator (red) and prey (blue) individuals. The smaller left patch (width  $L_{\perp}=100,$  carrying capacity K=1) resides in a stable active predator-prey coexistence state characterized by persistent radially propagating activity waves. The larger right subsystem ( $L_{\perp} = 200, K = 3$ ) is prone to fluctuation-driven total population extinction driven by initially abundant local predation events; as has happened by (b) t = 260 MCS(empty sites: black). Yet roughly planar invasion fronts emanating from both interfaces with the active region enter the empty, excitable subsystem, collide at (c) t = 800 MCS, generate wider population waves, and subsequently stabilize the vulnerable area in perpetuity at the higher species densities pertinent to K = 3, as shown at (d) t = 3000 MCS) [41, 45]. Time evolution of the population densities averaged over 21 independent runs in the (e) stable and (f) vulnerable regions.

istic LV activity fronts (left patch), whereas the population becomes extinct in the larger  $(200 \times 200)$  subsystem with K=3 (right). Yet at t=260 MCS one observes prey-predator fronts emanating from the stable environment to enter the empty patch, and as they propagate ballistically with speed v, revitalize it [41]. Indeed, the effect of the invasion waves may be viewed as a reset to correlated starting conditions that avoid large destabilizing population spikes. At t = 800 MCS, the two fronts collide and subsequently generate the dynamical quasi-stationary state characteristic for a (larger) stable LV system with K=3, viz. with higher population densities and wider activity waves than for K = 1. Graphs (e), (f) display the areal population densities  $n_{A/B}(t)$  in the stable (K=1) and vulnerable (K=3) regions. Remarkably, this stabilization through invasion waves into the inactive excitable domain remains effective essentially

independent of its size  $L_{\perp}$  provided it exceeds the typical wave front width  $\xi$ , and even stays intact when both regions are decoupled after elapsed time  $t_{\rm dec}$ , as long as a sufficient fraction of the vulnerable area is reactivated; i.e.,  $t_{\rm dec}$  is of the order of the traversal time  $t_{\rm inv}$  [41].

We next turn to basic epidemic processes [19] captured by the stochastic spatial SIS system [5, 15], where the infection spreads via the same predation reaction  $S+I \to I+I$  (probability  $\lambda$ ) as in the LV model, but with the birth/death processes replaced by the single recovery reaction  $I \to S$ , to which we assign a probability  $\gamma$ . Consequently, the total particle number and area density  $n_S + n_I$  remain conserved under this stochastic dynamics. Similar to the LV model, the SIS system features an active-to-absorbing transition in the DP universality class. The active phase permits repeated infection fronts spreading through the system. In this study, we fix  $\gamma = 0.1$ , restrict infection processes to neighboring square-lattice sites, and tune the infection probability close to the epidemic threshold  $\lambda_c \approx 0.108$ . Thus for  $\lambda = 0.115$ , even in small systems with linear extension L=100, the majority of simulation runs reaches the S-I coexistence state. Yet among 100 realizations initialized with a single (or a few) infectious I seed(s) surrounded by abundant susceptible individuals S, we found 27 runs to terminate at disease extinction,  $n_I \to 0$ . In contrast, for a slightly reduced infectivity  $\lambda = 0.109$ , all simulation runs are stochastically driven to the absorbing state where the infection wave dies out quickly.

As above for the LV system, in Fig. 3 we explore the ensuing stochastic dynamics in a heterogeneous combination of two now equally-sized square diffusively coupled SIS regions, respectively posited in the stable active epidemic state ( $\lambda = 0.115$ , left side) and a stochastic extinction-prone parameter range ( $\lambda = 0.109$ , on the right), each initiated with all sites occupied by susceptibles S (blue) except for a single I (red) individual placed at the subdomains' centers. In the run shown here, we separate and thus isolate both subsystems at t = 3000MCS. As expected, at t = 1300 MCS, one observes a near-threshold (fractal) spreading infection front on the left, whereas the infectious wave has terminated on the right. Once the epidemic wave reaches both interfaces to the inactive area, it incites invasion fronts that propagate into the excitable regions (t = 2900 MCS) and continue to do so at t = 4000 MCS even long after the diffusive coupling between the domains was shut down. Ultimately, both SIS subsystem reach their (quasi-)steady states with sustained epidemic spreading, but naturally a higher infection ratio in the patch with larger  $\lambda$  [45, 46].

An intriguing variation is explored in Fig. 4 where we diffusively couple the previous extinction-prone SIS system to a domain governed by the SIR model [5, 15, 36] stochastic processes  $S+I\to I+I$  (probability  $\lambda$ ) and  $I\to R$  (probability  $\gamma$ ), where no return from "recovered" to susceptible states  $R\to S$  is allowed. As a consequence,

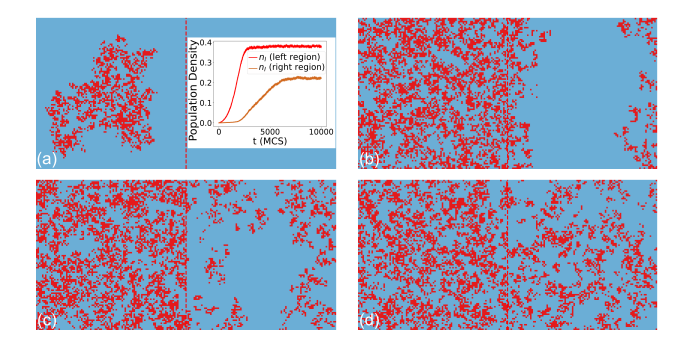


FIG. 3. Snapshots of a single Monte Carlo simulation run for two diffusively coupled SIS regions of equal size on a square lattice ( $L_{\parallel} = L_{\perp} = 100$ , periodic boundary conditions, carrying capacity K=1), initialized (t=0) with a single infectious (red) seed immersed in a susceptible (blue) population, subject to the infection probabilities  $\lambda = 0.115$  (left region),  $\lambda = 0.109$  (right subsystem) and recovery probability  $\gamma = 0.1$ , which sets the right patch very close to the epidemic threshold. (a) By t = 1300 MCS, the epidemic is spreading in the left subsystem, but has gone extinct on the right. The snapshots at (b) t = 2900 and (c) 4000 MCS show the infection fronts reaching the active region's boundaries and spreading into the inactive, susceptible domain (right); even though the diffusive coupling was turned off at t = 3000 MCS. (d) In the (quasi-)stationary regime (t = 6000 MCS), both isolated regions sustain the epidemic outbreak, with a lower infectious population density  $n_I$  on the right. The inset in (a) shows the temporal increase of  $n_I(t)$  in both subsystems (averaged over the surviving runs in the more robust left ecosystem) [45, 46].

only a *single* epidemic wave can be sustained in the SIR system, and the infection ultimately dies out irrespective of the model parameters. We again combine two square SIR and SIS subsystems of the same linear size L = 100 initiated (t = 0) with a single active I (red) site each; on the SIS side (right), we set  $\lambda = 0.109$  and  $\gamma = 0.1$ . For the SIR region, we impose  $\lambda = 0.210$  and  $\gamma = 0.1$ , which allows the epidemic wave to spread across the entire domain. In this Monte Carlo run, the infection has gone extinct by t = 400 MCS in the SIS patch. At t = 1000 MCS, the SIR epidemic front spreading on the left patch, leaving in its wake large recovered areas (black) with smaller untouched susceptible (blue) enclosures, has reached the interfaces to the SIS subsystem, spawning planar infection waves that invade the excitable SIS domain. By t = 2000 MCS, the SIR outbreak has ceased, terminating the transient excitations across the boundaries to the SIS side; still the epidemic there keeps spreading and eventually reaches its (quasi-)stationary state. In an analogous manner, the single outbreak in an SIR region where the infection front can reach across the entire system can trigger an epidemic in a diffusively coupled SIR patch with lower infectivity for which a single active I seed could not spawn a spreading front [45, 46].

The above stabilization mechanism of finite spatially extended systems prone to be driven stochastically to an

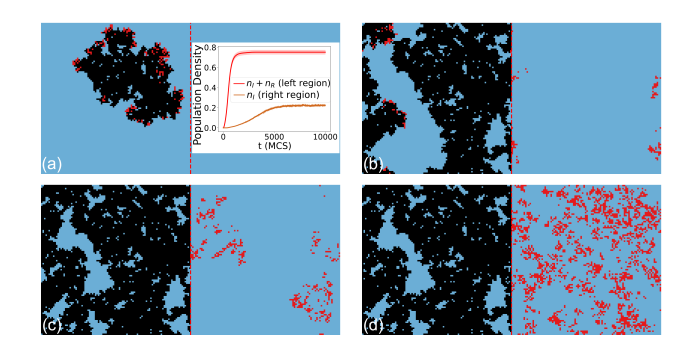


FIG. 4. Snapshots of a single Monte Carlo simulation run for two diffusively coupled SIR (left) and SIS (right) systems of equal size on a square lattice ( $L_{\parallel}=L_{\perp}=100,$  periodic boundary conditions, carrying capacity K = 1), initialized (t=0) with a single infectious (red) seed immersed in a susceptible (blue) population, subject to the infection probabilities  $\lambda = 0.210$  (left region),  $\lambda = 0.109$  (right) and recovery probability  $\gamma = 0.1$  (on the left, recovered individuals are indicated black). (a) At t = 400 MCS, the epidemic is spreading in the left SIR patch, but has gone extinct on the SIS side. (b) The snapshot at t = 1000 MCS depicts incipient infection fronts emanating from the interfaces and invading into the inactive susceptible SIS region (right). (c) By t = 2000MCS steps, the outbreak has run its course in the SIR region and reached its final state with a majority of recovered sites (black) interspersed by untouched susceptible (blue) patches, while the epidemic continues to spread in the SIS domain. (d) At longer run times (here t = 6000 MCS), both effectively decoupled systems persist in their respective (quasi-)stationary states, with infection events occurring continuously and persistently in the right SIS patch. The inset in (a) shows the population densities  $n_I + n_R$  (left region) and  $n_I$  (right) [45, 46].

absorbing state is not restricted to hierarchical binary interaction schemes. Indeed, consider the three-species ML cyclic competition model [43], defined by the stochastic predation and reproduction reactions  $S_i + S_{i+1} \rightarrow S_i$ (probability  $\lambda_i$ ),  $S_i \rightarrow S_i + S_i$  (probability  $\sigma_i$ ), with species indices i = 1, 2, 3 and i + 3 to be identified with i. For large enough extension, the ML model displays spontaneously emerging spiral structures that stabilize species coexistence [14]. Yet when the typical spiral size reaches the system boundaries, this spatial "advantage" disappears, the model effectively becomes zero-dimensional and susceptible to stochastic fixation events, leaving just a single species [11]. This vulnerability against two-species extinction is enhanced in strongly asymmetric ML models (e.g., setting  $\lambda_1 \gg \lambda_2 = \lambda_3$  or  $\lambda_1 \ll \lambda_2 = \lambda_3$ ), for which the stochastic trajectories approach the absorbing edges in parameter space (akin to heteroclinic cycles in mean-field theory). As demonstrated in Ref. [47], diffusively coupling an asymmetric cyclic ML three-species ecology with an even much smaller stable one (viz., with symmetric reactivities) incites planar invasion fronts at the subsystems' interfaces that in turn generate spiral structures in the bulk of the vulnerable region and thereby re-animate all three competing populations.

Illustrated by several paradigmatic models from ecology, epidemiology, and game theory, we have demonstrated that instabilities against stochastic extinction or fixation can be effectively countermanded by diffusively coupling the vulnerable subsystem to an even much smaller stable region. Originating at the interfaces, influx through immigration waves effectively resets initial conditions and suffices to maintain activity across the entire system, even when the two patches are eventually decoupled. We emphasize that this boundary-driven stabilization should be a quite generic phenomenon in finite complex systems tending towards an absorbing state. The basic requirements for this mechanism only appear to be that (1) typical extinction times depend sensitively on system size; (2) the source region stays stable during the time period when both subsystems are diffusively coupled; and (3) the absorbing region remains "excitable", i.e., capable of sustaining traveling invasion fronts. Hence we expect this intriguing scenario to be broadly applicable to a wide range of natural phenomena.

We gratefully acknowledge helpful discussions with Erwin Frey and Michel Pleimling. We are indebted to Shannon Serrao and Canon Zeidan for providing unpublished preliminary data on their May—Leonard model Monte Carlo simulations. This research was partly supported by the U.S. National Science Foundation, Division of Mathematical Sciences under Award No. NSF DMS-2128587.

- \* dkenneth@vt.edu
- † sarashabani@vt.edu
- <sup>‡</sup> tauber@vt.edu; Faculty of Health Sciences, Virginia Tech
- [1] N. G. van Kampen, Stochastic Processes in Physics and Chemistry (North Holland, Amsterdam, 1981).
- [2] K. Lindenberg, R. Metzler, and G. Oshanin (eds.), Chemical Kinetics Beyond the Textbook (World Scientific, Singapore, 2020).
- [3] R. M. May, Stability and Complexity in Model Ecosystems (Princeton University Press, Princeton, 1973).
- [4] J. Hofbauer and K. Sigmund, Evolutionary Games and Population Dynamics (Cambridge University Press, Cambridge, 1998).
- [5] M. Keeling and P. Rohani, Modeling Infectious Diseases in Humans and Animals (Princeton University Press, Princeton, 2011).
- [6] R. L. Jack, J. P. Garrahan, and D. Chandler, J. Chem. Phys. 125, 184509 (2006).
- [7] M. Kohl, R. F. Capellmann, M. Laurati, S. U. Egelhaaf, and M. Schmiedeberg, Nature Comm. 7, 11817 (2016).
- [8] A. Deger, A. Lazarides, and S. Roy, Phys. Rev. Lett. 129, 190601 (2022).
- [9] K. A. Takeuchi, M. Kuroda, H. Chaté, and M. Sano, Phys. Rev. Lett. 99, 234503 (2007).
- [10] H. Y. Shih, T. L. Hsieh, and N. Goldenfeld, Nature Phys. 12, 245 (2016).

- [11] Q. He, M. Mobilia, and U. C. Täuber, Phys. Rev. E 82, 051909 (2010); Eur. Phys. J. B 82, 97 (2011).
- [12] A. Dobrinevski and E. Frey, Phys. Rev. E 85, 051903 (2012).
- [13] R. Durrett, SIAM Review 41, 677 (1999).
- [14] T. Reichenbach, M. Mobilia, and E. Frey, Nature 448, 1046 (2007).
- [15] J. D. Murray, Mathematical Biology, Vols. I & II (Springer, New York, 3rd ed. 2002 / 2003).
- [16] M. Cross and H. Greenside, Pattern Formation and Dynamics in Nonequilibrium Systems (Cambridge University Press, Cambridge, 2009).
- [17] M. Mobilia, I. T. Georgiev, and U. C. Täuber, J. Stat. Phys. 128, 447 (2007).
- [18] T. Butler and N. Goldenfeld, Phys. Rev. E 80, 030902(R) (2009); Phys. Rev. E 84, 011112 (2011).
- [19] U. C. Täuber, Critical Dynamics (Cambridge University Press, Cambridge, 2014).
- [20] U. Dobramysl, M. Mobilia, M. Pleimling, and U. C. Täuber, J. Phys. A: Math. Theor. 51, 063001 (2018).
- [21] U. C. Täuber, in Order, Disorder, and Criticality, Vol. VIII, Y. Holovatch (ed.), Chap. 2, p. 67 (World Scientific, Singapore, 2024).
- [22] H. K. Janssen, Z. Phys. B Cond. Matt. 42, 15 (1981).
- [23] P. Grassberger, Z. Phys. B Cond. Matt. 47, 365 (1982).
- [24] H. Hinrichsen, Adv. Phys. 49, 815 (2000).
- [25] G. Ódor, Rev. Mod. Phys. 76, 663 (2004).
- [26] M. Henkel, H. Hinrichsen, and S. Lübeck, Non-equilibrium Phase Transitions, Vol. 1: Absorbing Phase Transitions (Springer, Dordrecht, 2008).
- [27] U. C. Täuber, Annu. Rev. Condens. Matt. Phys. 8, 14 (2017).
- [28] H. K. Janssen, Phys. Rev. Lett. 78, 2890 (1997).
- [29] T. E. Harris, Ann. Prob. 2, 969 (1974).
- [30] J. Marro and R. Dickman, Nonequilibrium Phase Transitions in Lattice Models (Cambridge University Press, Cambridge, 1999).
- [31] H. Matsuda, N. Ogita, A. Sasaki, and K. Satō, Prog. Theor. Phys. 88, 1035 (1992).
- [32] J. E. Satulovsky and T. Tomé, Phys. Rev. E 49, 5073 (1994).
- [33] A. Lipowski and D. Lipowska, Physica A **276**, 456 (2000).
- [34] R. Monetti, A. Rozenfeld, and E. Albano, Physica A 283, 52 (2000).
- [35] T. Antal and M. Droz, Phys. Rev. E 63, 056119 (2001).
- [36] W. O. Kermack, A. G. McKendrick, and G. T. Walker, Proc. R. Soc. A 115, 700 (1927).
- [37] P. Grassberger, Math. Biosci. **63**, 157 (1983).
- [38] J. L. Cardy and P. Grassberger, J. Phys. A: Math. Gen. 18, L267 (1985).
- [39] T. Tomé and R. Ziff, Phys. Rev. E. 82, 051921 (2010).
- [40] M. Swailem and U. C. Täuber, Phys. Rev. E 107, 064144 (2023).
- [41] K. Distefano and U. C. Täuber, in preparation (2025).
- [42] B. Heiba, S. Chen, and U. C. Täuber, Physica A 491, 582 (2018).
- [43] R. M. May and W. J. Leonard, SIAM J. Appl. Math. 29, 243 (1975).
- [44] M. L. Arnau, S. R. Serrao, and U. C. Täuber (2020).
- [45] For simulation movies of various stochastic models, see: www.phys.vt.edu/~tauber/PredatorPrey/InhSta/.
- [46] S. Shabani and U. C. Täuber, in preparation (2025).

[47] S. R. Serrao and U. C. Täuber, Eur. Phys. J. B 94, 175 (2021).